X-ray diffraction Studies of Cr^{3+} Substituted Nanocrystalline Cobalt Manganese Ferrites

M. M. Langade and D. V. Mane*

Department of Chemistry, Jawahar Art, Science and Commerce College Andur.(M.S.)

Deputy Director, UGC – Academic Staff College ,Dr.Babasaheb Ambedkar Marathwada University,Aurangabad

**Corresponding Author*

Abstract: Single phase cubic spinal nanocrystalline ferrites having composition $CoMn_{1-x}Cr_xFeO_4$, with varying concentration of chromium (x=0.00,0.25,0.50.0.75 and1.00) were synthesized by sol-gel method, resulting single phase cubic spinals.The unit cell parameter decreased with increase in Cr^{3+} substitution.T.E.M studies revealed the nanocrystalline nature of the synthesized samples. I.R absorption spectra of all investigated ferrite samples shown two strong absorption bands in the range of 716-748 cm^{-1} , due to intrinsic vibrations of the tetrahedral group, and second band in the range of 294-375 cm^{-1} due to octahedral metal complexes. The magnetic properties were measured by vibrating sample magnetometer which showed that the saturation magnetization decreased with increase in concentration of Cr^{3+} ion, due to weaker magnetic moment of Cr^{3+} ion as compared to Mn^{3+}ions.

Key words: Nanocrystalline magnetic material, sol-gel synthesis, TEM, X-ray analysis,

Introduction

Cobalt ferrite ($CoFe_2O_4$) corresponds to the group of spinel-type ferrites, which are compounds with a cubic oxygen lattice of the general formula $Me_xFe_{3-x}O_4$ [1], where Me is usually a divalent metal cation. The properties of ferrites depend mainly upon chemical composition, method of preparation, sintering time and temperature [2]. Introducing small amount of a foreign ion can change the electrical and magnetic properties of the ferrite [3]. $CoMn_{1-x}Cr_xFeO_4$ spinel ferrite nano particulate system may offer an opportunity to study the roles of Co^{2+}, Mn^{3+} and Fe^{3+} in spinel ferrites through the variation of Cr^{3+} ion concentration. The wide applications of nano crystalline ferrites lead to the development of

various synthesis methods, which include hydrothermal, ultrasonically assisted hydrothermal, mechanical alloying, pulsed wire discharge, shockwave, reverse micelle co-precipitation, freeze drying, spray drying, precursor and sol–gel [4-6]. The sol–gel method, in particular, is one of the most useful and attractive techniques for the synthesis of nano crystalline ferrite materials because of its advantages such as; good stoichiometric control and the production of nanocrystalline particles.

Experimental

Analytical grade reagents, cobalt nitrate ($Co(NO_3)_2 \cdot 3H_2O$), chromium nitrate ($Cr(NO_3)_3 \cdot 9H_2O$), manganese nitrate ($Mn(NO_3)_2 \cdot 6H_2O$),iron nitrate ($Fe(NO_3)_3 \cdot 9H_2O$) and citric acid ($C_6H_8O_7 \cdot H_2O$),were used to synthesize the $CoMn_{1-x}Cr_xFeO_4$ (x = 0.0, 0.25, 0.5, 0.75, 1.0) ferrite nanoparticles. In the present study, sol-gel auto-combustion method was adopted to synthesize the ferrite nanoparticles. Reaction procedure was carried out in air atmosphere without protection of inert gases. The molar ratio of metal nitrates to citric acid was taken as 1:3. The metal nitrates were dissolved together in a minimum amount of double distilled water to get a clear solution. An aqueous solution of citric acid was mixed with metal nitrates solution, then ammonia solution was slowly added to adjust the pH at 7. Then the solution was heated at 90ºC to transform into gel. When ignited at any point of the gel, the dried gel burnt in a self-propagating combustion manner until all gel was completely burnt out to form a fluffy loose powder. The auto-combustion was completed within a minute, yielding the brown-colored ash termed as a precursor. It has been observed that the calcinations temperature is an important parameter during the synthesis of ferrite nanoparticles via sol–gel method which affects the physical and magnetic properties of ferrite nanoparticles. Therefore, the as prepared ferrite powder was annealed at 600 ºC for 4 h in order to compete the crystallization.

The crystal structure of the as-prepared samples was characterized by X-ray diffraction technique using Phillips X-ray diffractometer (Model 3710) equipped with Cu-K_α radiation (λ=1.5405Å). The microstructure was examined on the fracture surfaces of the samples using thermal field emission

scanning electron microscope (SEM). Transmission electron microscope (TEM) measurements were recorded on Philips (Model CM 200). Infrared spectra of all the samples were recorded at room temperature in the range 300 cm^{-1} to 800 cm^{-1} using Perkin Elmer infrared spectrophotometer. Room temperature magnetization of the samples was measured using the pulse field magnetization set-up.

Results and discussion

Structural Analysis

Fig.1. shows X-ray diffraction pattern for all the investigated samples. The indexing the XRD pattern indicates the nominal composition structure is single-phase cubic spinel structure with Fd^3m cubic spinel space group. The reflection from the planes, (2 2 0), (3 1 1), (2 2 2), (4 0 0), (4 2 2), (3 3 3) and (4 4 0) appeared for all samples.

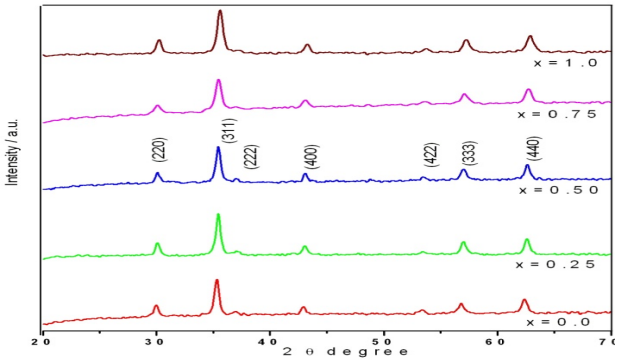

Fig. 1.X-Ray diffraction patterns of for $CoMn_{1-x}Cr_xFeO_4$(x=0.00,0.25,0.50.0.75 and 1.00)

The values of lattice parameter (*a*) were obtained by fitting the diffracted peaks using standard least-squares method and by employing eq. 1 are listed in Table .1.

$$a = d\sqrt{N} \qquad \sqrt{N} = \sqrt{\left(h^2 + k^2 + l^2\right)} \qquad \textbf{1}$$

Where *d* is the inter-planer spacing and (*hkl*) is the index of XRD reflection peak.

The variation of lattice constant with increasing Cr^{3+}substitution can be explained on the basis of difference in ionic radii of Mn3+ (0.80 Å)replaced by Cr^{3+} (0.63Å,its results the lattice shrinks and the lattice constant decreases.

The X-ray density (dx) of all the samples of the series obtained by the following relation is presented in Table .1.

$$dx = \frac{8M}{Na^3} \qquad \mathbf{2}$$

where '8' is the number of molecules per unit cell, 'M' is the molecular weight of sample, 'N' is the Avogadro's number and 'a' is lattice constant.

X-ray density increases with increase Cr^{3+} concentration, while the lattice parameter (*a*) shows opposite behavior. This causes a decrease in the size of the unit cell and consequently, it causes an increase of the X-ray density. Secondly the variation may be related to the difference in the atomic weights between Cr^{3+} and Mn^{3+} ions.

The crystallite size of the nanocrystalline samples were measured from XRD line broadening analysis applying Scherrer's formula [3]:

$$D_{XRD} = \frac{k\lambda}{\beta \cos\theta} \qquad \mathbf{3}$$

Where D_{XRD} is the dimension of the crystallite, λ is wavelength of the X-ray radiation, θ is the Bragg angle, k is a shape factor taken to be 0.94 and β is peak width measured at half of the maximum intensity.

Crystallite size (D_{XRD}) from the XRD data was determined by using the Scherer formula (eq.3) [45]. The peaks of (2 2 0), (3 1 1), (2 2 2), (4 0 0), (4 2 2), (3 3 3) and (4 4 0) were deconvoluted to Lorentzian curves for the determination of the crystallite size using full-width at half maximum value. It is observed from Table 1. that the D_{XRD} decreased from 19.8 (x = 0.0) to 14.1 nm for x = 0.5 and it again increased to 16.3 nm for x = 1.0. It can be concluded that the replacement of Mn^{3+} ions with Cr^{3+} in Co–Mn ferrite may lead to a decrease in cation vacancies and in turn to a decrease of crystallite size.

The percentage porosity (P) calculated using the following relation is tabulated in Table 1.

$$P = \left(\frac{d_X - d_B}{d_X}\right) \times 100 \qquad \mathbf{4}$$

Where d_x and d_B are the X-ray density and bulk density respectively.

Table.1. Lattice constant (a), X-ray density (d_x), crystallite size (D_{XRD}), bulk density (d_B) and porosity (P) of $CoMn_{1-x}Cr_xFeO_4$.

Comp. x	a (Å)	dx (g/cm^3)	D_{XRD} (nm)	d_B (g/cm^3)	P (%)
0.00	8.3972	5.243	19.8	4.121	21.41
0.25	8.3882	5.244	18.5	4.112	21.58
0.50	8.3717	5.258	14.1	4.109	21.86
0.75	8.3588	5.266	16.6	4.107	22.01
1.00	8.3566	5.273	16.3	4.107	21.82

The Cr^{3+} substitution enhance the porosity thus decreasing the density of the sample. Since the decrease of bulk density is in order 0.014 g/cm^3 with Cr substitution while the increase of X-ray density for x=0.0 to x=0.75 is of order 0.022g/cm^3, one can expect the porosity to increase with increasing Cr substitution

In order to investigate the particle morphology and confirm the phase structure of the sol-gel synthesized Co-Mn ferrite nano particle samples, selected samples were examined by high magnification TEM. The results are also helpful in order to clarify the nanostructure of ferrite magnetic nanoparticles prepared by sol-gel method. It is observed from Fig.2, that magnetic nanoparticles are aggregated.

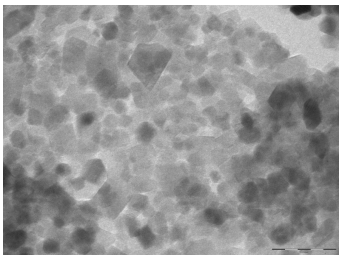

Fig. 2. Transmission electron micrograph (TEM) image of x = 1.0 (Average particle size 15nm) for $CoMn_{1-x}Cr_xFeO_4$

The average values of the nanocrystalline particles are consistent with the result obtained from XRD analysis. It is evident that the magnetic nanoparticles are not exactly spherical in shape. With the observation of ferrite nanoparticles, the shape of the spinel crystal is cubic structure. It can also be seen from TEM images that the ferrite nano particles are uniform in both morphology and particle size, but agglomerated to some extend due to the interaction between magnetic nanoparticles.

It has been reported that the hopping length 'L_A and L_B' (i.e. the distance between the magnetic ions) of electrons influences the physical properties of the ferrite system. Hopping of electrons between B- and A-sites is less probable compared to that between B- and B-sites, because the distance between the two metal ions placed in B-sites is smaller than when one in B-sites and the other in A-sites.

L_A and L_B i.e. the hopping length for tetrahedral A- and octahedral B-sites respectively were calculated using the following relation:[5,6]

$$L_A = a\sqrt{\frac{3}{4}} \quad \textbf{5}$$

$$L_B = a\sqrt{\frac{2}{4}} \quad \textbf{6}$$

Substituting the experimental values of lattice constant '*a*', oxygen positional parameter '*u*' (0.375 Å) in following equations, the allied parameters such as tetrahedral and octahedral bond length (d_{Ax} and d_{Bx}), tetrahedral edge, shared and unshared octahedral edge (d_{AXE}, $d_{BXE,}$ d_{BXES} and d_{BXEU}) were calculated [7-11].

$$d_{AX} = a\sqrt{3}\left(u - \frac{1}{4}\right) \quad \textbf{7}$$

$$d_{BX} = a\left[3u^2 - \left(\frac{11}{4}\right)u + \frac{43}{64}\right]^{\frac{1}{2}} \quad \textbf{8}$$

$$d_{AXE} = a\sqrt{2}\left(2u - \frac{1}{2}\right) \quad \textbf{9}$$

$$d_{BXEshaired} = a\sqrt{2}\left(1 - 2u\right) \quad \textbf{10}$$

$$d_{BXEunshaired} = a\left(4u^2 - 3u + \frac{11}{16}\right)^{\frac{1}{2}} \quad \textbf{11}$$

All the allied parameters; tetrahedral and octahedral bond length (d_{Ax} and d_{Bx}), tetrahedral edge, shared and unshared octahedral edge (d_{AXE} and d_{BXE}) were calculated using equations 10&11. The values of all the allied parameters are tabulated in Table 2. It is observed that d_{Ax}, d_{Bx}, d_{AXE} and d_{BXE} decrease with increasing Cr^{3+} substitution. This is due to the substitution process, that is, replacement of larger

ionic radii (Mn^{3+}) by smaller ionic radii (Cr^{3+}) and their distribution over the tetrahedral A- and octahedral B-sites.

Table.2 Hopping lengths (L_A and L_B), Tetrahedral bond (d_{AX}), octahedral bond (d_{BX}), tetra edge (d_{AXE}) and octahedral edge (d_{BXE}) (shared and unshared) of $CoMn_{1-x}Cr_xFeO_4$

Comp. x	Hopping length		d_{AX} (Å)	d_{BX} (Å)	Tetra edge (Å)	Octa edge d_{BXE} (Å)	
	L_A (Å)	L_B (Å)				Shared	unshared
0.00	3.6361	2.9689	1.905	2.052	3.111	2.826	2.976
0.25	3.6322	2.9657	1.903	2.050	3.108	2.823	2.973
0.50	3.6251	2.9598	1.899	2.046	3.101	2.817	2.967
0.75	3.6195	2.9553	1.897	2.043	3.097	2.813	2.963
1.00	3.6185	2.9545	1.896	2.042	3.096	2.812	2.962

Conculsion:

The present system prepared bt sol gel auto combustion method which yielding in the range of 14 -19 nm particle size. X-ray diffraction of all the sample exhibits formation of single phase cubic structure. The lattice constant decrease with increase in Cr^{3+} content, which attributed to the difference ionic radii of the constituents ions. Hopping length,(L_A, L_B) tetrahedral and octahedral edges also decreases with replacement of larger Mn^{3+} ions by Cr^{3+} ions.

References:

[1] V. N.Antonov, B. N.Harmon, V. P.Antropov, A. Y. Perlov,A. N. Yresko, Phys. Rev. B 64 (2001) 134410.

[2] Sagar E Shirsath, "Synthesis condition reflected structural and magnetic properties of $Li_{05}Cr_{05}Fe_2O_4$ nanoparticles" in 'Magnetic Nanoparticles: Properties, Synthesis and Applications' edited by Beate Acklin and Edon Lautens, Nova publishers, New York,2012.

[3] Sagar E. Shirsath, Yukiko Yasukawa, Ali Ghasemi, Xiaoxi Liu, and Akimitsu Morisako, J. Appl. Phys. 115 (2014) 17A515

[4] Y. Kinemuchi, K. Ishizaka, H. Suematsu,W. Jiang, K. Yatsui, Thin Solid Films 407(2002) 109.

[5] J. Zhou, J. Ma, C. Sun, L. Xie, Z. Zhao, H. Tian, J. Am. Ceram. Soc. 88 (2005) 3535.

[6] P.E. Meskin, V.K. Ivanov, A.E. Barantchikov, B.R. Churagulov, Y.D. Tretyakov,Ultrason. Sonochem. 13 (2006) 4.

[7] B. D. Cullity, Elements of X-ray diffraction, Addison-Wesley, London, 1959.

[8] R.Valenzuela, Magnetic ceramics, Cambridge University Press, 1994.

[9] R.H.Kadam, Kirti Desai, Suprya R. Kadam, Sagar E. Shirsath,Solid State Science,2692013)31-37

[10] R.D. Waldron, Phys. Rev. 99 (1955) 1727.

[11] S.A.Patil, S.M.Otari, V.C.Mahajan, A.B.Patil et al. Solid StateCommun.78(1) (1991) 39.

[12] S.A. Mazen, M.H. Abdallah, B.A. Sabrah, H.A.M. Hashem, Phys.Stat. Sol. (a) 134 (1992) 263–271.

[13] A.M. El-Sayed, Ceram. Inter. 28 (2002) 651–655.

[14] E.C. Stoner and E.P. Wohlfarth, Phil. Trans. Roy. Soc. A 240 (1948)599; Reprinted by IEEE Trans. Magn. 27 (1991)3475.

[15] S. H. Liou, S. Huang, E. Klimek, and R. D. Kirby, J. Appl. Phys. 85, 4334 (1999)

[16] P.K. Roy, J. Bera, J. Magn. Magn. Mater. 320 (2008) 1128.

[17] Sagar E. Shirsath, R. H. Kadam, Anil S. Gaikwad, Ali Ghasemi, Akimitsu Morisako, J. Magn. Magn. Mater.323 (2011) 3104–3108